

An In-Depth Spectroscopic Analysis of the Blazhko Star RR Lyr [★]

I. Characterisation of the star: abundance analysis and fundamental parameters

K. Kolenberg¹, L. Fossati², D. Shulyak³, H. Pikall¹, T.G. Barnes⁴, O. Kochukhov⁵, and V. Tsymbal⁶

¹ Institut für Astronomie, Universität Wien, Türkenschanzstrasse 17, 1180 Wien, Austria.
e-mail: katrien.kolenberg@univie.ac.at, holger.pikall@univie.ac.at

² Department of Physics and Astronomy, Open University, Walton Hall, Milton Keynes, MK7 6AA, UK.
e-mail: l.fossati@open.ac.uk

³ Institute of Astrophysics, Georg-August-University, Friedrich-Hund-Platz 1, D-37077, Göttingen, Germany.
e-mail: denis.shulyak@gmail.com

⁴ The University of Texas at Austin, McDonald Observatory, 1 University Station, C1402, Austin, Texas, 78712-0259, USA.
e-mail: tgb@astro.as.utexas.edu

⁵ Department of Astronomy and Space Physics, Uppsala University, 751 20, Uppsala, Sweden.
e-mail: oleg@astro.uu.se

⁶ Tavrian National University, Vernadskiy's Avenue 4, Simferopol, Crimea, 95007, Ukraine.
e-mail: vadim.tsymbal@gmail.com

ABSTRACT

Aims. The knowledge of accurate stellar parameters is a keystone in several fields of stellar astrophysics, such as asteroseismology and stellar evolution. Although the fundamental parameters can be derived both from spectroscopy and multicolour photometry, the results obtained are sometimes affected by systematic uncertainties. In this paper, we present a self-consistent spectral analysis of the pulsating star RR Lyr, which is the primary target for our study of the Blazhko effect.

Methods. We used high-resolution and high signal-to-noise ratio spectra to carry out a consistent parameter determination and abundance analysis for RR Lyr. The LLMODELS code was employed for model atmosphere calculations, while SYNTH3 and WIDTH9 codes were used for line profile calculation and LTE abundance analysis. We provide a detailed description of the methodology adopted to derive the fundamental parameters and the abundances. Stellar pulsation reaches high amplitudes in RR Lyrae stars, and as a consequence the stellar parameters vary significantly over the pulsation cycle. The abundances of the star, however, are not expected to change. From a set of available high-resolution spectra of RR Lyr we selected the phase of maximum radius, at which the spectra are least disturbed by the pulsation. Using the abundances determined at this phase as a starting point, we expect to obtain a higher accuracy in the fundamental parameters determined at other phases.

Results. The set of fundamental parameters obtained in this work fits the observed spectrum accurately. Through the abundance analysis, we find clear indications for a depth-dependent microturbulent velocity, that we quantified.

Conclusions. We confirm the importance of a consistent analysis of relevant spectroscopic features, application of advanced model atmospheres, and the use of up-to-date atomic line data for the determination of stellar parameters. These results are crucial for further studies, e.g., detailed theoretical modelling of the observed pulsations.

Key words. Stars: abundances – Stars: fundamental parameters – Stars: individual: RR Lyr

1. Introduction

The modelling of pulsational signals requires the knowledge of stellar parameters and primarily accurate values of the effective temperature (T_{eff}) and metallicity (Z). The determination of fundamental parameters can be performed by different methods (some examples for stars from B- to G- type are Fuhrmann et al. 1997, Przybilla et al. 2006, and Fossati et al. 2009) that do not always lead to consistent results. Thus, it is important to choose a methodology that allows us to constrain the parameters of the star from the available observables (usually photometry and spectroscopy) in the most robust and reliable way.

RR Lyr is the prototype and eponym of its class of pulsating stars. RR Lyrae stars play a crucial role as distance indicators. Their evolutionary stage (He burning in core, H burning in shell) makes them useful tracers of galactic history. These

classical pulsators display radial oscillations (the simplest type of pulsation) with large amplitudes which makes them useful touchstones for theoretical modelling. RR Lyr is one of the best studied stars of its class. Almost a century ago Shapley (1916) discovered that it shows a strong Blazhko effect, i.e. a (quasi-)periodic modulation of its light curve shape in amplitude and phase. The Blazhko effect in RR Lyr has been closely followed over the past century, and changes have been reported both in the strength and the duration of its Blazhko cycle (Szeidl 1988, Kolenberg et al. 2006). Some well-studied stars even show multiple (variable) modulation periods (see, e.g., LaCluyzé et al. 2004). Despite numerous attempts to model the phenomenon, the Blazhko effect has eluded a satisfactory explanation so far. Recently obtained high-precision photometry from ground-based or space-borne precise instruments also indicate that Blazhko modulation may be a much more common phenomenon than initially thought: as many as half of galactic

[★] Data obtained with the 2.7-m telescope at McDonald Observatory, Texas, US

RRab stars may be modulated (Jurcsik et al. 2009; Szabo et al. 2009; Kolenberg et al. 2010).

In order to constrain the viable models for the Blazhko effect, it is vital to obtain accurate values for the fundamental parameters (and their variations) for modulated and non-modulated RR Lyrae stars. This has been the main motivation for the study presented in this article.

RR Lyr is the only star of its class to have a directly determined parallax, recently measured with the HST/FGS, by Benedict et al. (2002), to be $\pi(\text{FGS}) = 3.82 \pm 0.2$ mas ($d = 262 \pm 13$ pc). When a small ISM correction of $A_v = 0.07$ is applied, this new distance results in an $M_v^{\text{RR}} \approx +0.61_{-0.11}^{+0.10}$ mag which corresponds to $\approx 49 \pm 5L_{\odot}$.

Fundamental parameters of RR Lyr have been obtained by several authors with a variety of methods (e.g., Lambert et al. 1996; Manduca et al. 1981; Siegel 1982; for a summary see Kolenberg 2002). The published fundamental parameters of RR Lyr display a considerable range both in T_{eff} and $\log g$ due to the large pulsation amplitudes. According to these analyses, RR Lyr's T_{eff} varies over its 13h36min pulsation cycle between approximately 6250 and 8000 K and its $\log g$ between 2.5 and 3.8 (extreme values). Superposed on the large variation, the Blazhko cycle leads to an additional variation of the fundamental parameters. Jurcsik et al. (2008) recently showed that also the *mean* properties of modulated RR Lyrae stars change over the Blazhko cycle. Element abundances of RR Lyr were obtained previously by, e.g., Clementini et al. (1996), Lambert et al. (1996), and Takeda et al. (2006).

The main goal of the present work is to perform a self-consistent atmospheric and abundance analysis of RR Lyr that reproduces all of its photometric and spectroscopic data. Furthermore, we want to investigate the degree to which the derived fundamental parameters depend on the applied methods. Considering the structure of the available models, especially the position of the convective zones and the zones of nuclear fusion, the measured abundances of the star are not expected to change over the pulsation (and the Blazhko) cycle. Hence, if the abundances are accurately determined at one phase in the pulsation cycle, they can be of help to determine (or at least constrain) the fundamental parameters at other phases. In this paper we also selected the optimal phase for determining the abundances of the star. This is the first of a series of planned papers devoted to a detailed spectroscopic study of RR Lyr. In forthcoming papers we will discuss the spectral variations over the pulsation and Blazhko cycle of the star.

2. Observations and spectral data reduction

A total of 64 spectra of RR Lyr were obtained between June 26th and August 27th, 2004 with the Robert G. Tull Coudé Spectrograph on the 2.7-m telescope of McDonald Observatory. This is a cross-dispersed échelle spectrograph yielding a two-pixel resolving power $R \approx 60000$ for the configuration used here. Table 1 lists the observing time, exposure time, the S/N ratio per resolution element for each acquired spectrum, and the phases in the pulsation and Blazhko cycles. For the determination of the phases we used the ephemerides derived by Kolenberg et al. (2006). To minimize smearing of the spectral features by pulsation, each spectrum was limited to an exposure time of 960 seconds. Two spectra have shorter exposures as a result of being stopped due to cloud. The signal-to-noise ratio (SNR) per resolution element of the obtained spectra varies according to the brightness of the star (given the fixed integration time) and the weather conditions during the observation. Spectra ID319-328

were inadvertently taken at the wrong blaze angle and thus have poor S/N ratios.

Bias frames and flat-field frames were obtained at the start of each night, and Th-Ar spectra were observed frequently during each night for calibration purposes. The spectra were reduced using the Image Reduction and Analysis Facility (IRAF¹, Tody 1993). Each spectrum, normalised by fitting a low order polynomial to carefully selected continuum points, covers the wavelength range 3633-10849 Å, with several gaps between the orders at wavelengths greater than 5880 Å.

The normalisation of the hydrogen lines was a crucial point since we used them as source for the derivation of the T_{eff} . $H\alpha$ was not covered by our spectra, and the orders adjacent to $H\beta$ were affected by a spectrograph defect which hindered a proper normalization. We were able to perform a reliable normalisation of the $H\gamma$ line using the artificial flat-fielding technique described by Barklem et al. (2002). This approach assumes that the relation between the blaze shapes of the different échelle orders is a smoothly changing function of the order number. On this basis one can establish the apparent blaze shapes by fitting polynomials to continuum points in several orders above and below the hydrogen line. On the subsequent step a 2-D polynomial surface is fitted to these empirical blaze functions, and the continuum in the orders containing the $H\gamma$ line is determined by interpolation.

This normalisation procedure was performed on two spectra taken near the optimal phase. We used a surface fit to 3–4 orders on both sides of the broad hydrogen line to determine the continuum in the $H\gamma$ spectral orders. The accuracy of this normalisation technique is attested by a good agreement between the normalised overlapping $H\gamma$ profiles and by the lack of discrepancy between observations of RR Lyr obtained at similar pulsation phases.

Simultaneously with the spectroscopic campaign, we obtained photometric data in Johnson *V* through a multi-site campaign. The photometric data were published by Kolenberg et al. (2006). They were used for accurate determination of the pulsation frequencies and phases in the pulsation and Blazhko cycle.

3. The models

3.1. The pulsation model

In order to determine the dynamical properties of the atmosphere at the most quiescent phases theoretically, we used the so-called Vienna Nonlinear Pulsation Code. For the unperturbed starting model we utilized the values of $0.65M_{\odot}$ and $50L_{\odot}$ together with $T_{\text{eff}} = 6600\text{K}$ and a typical Pop II chemical composition of $Y = 0.239$ and $Z = 0.001$ which lead to a limit cycle with the observed period of pulsation. The kinetic energy of the atmosphere (defined as the part from the photosphere where $\tau = 2/3$ to the outer boundary of our model, see Fig. 1) shows 2 local minima, where the first – roughly at phase 0.35 – corresponds to the phase of maximum photospheric radius. The flow ceases and the whole envelope starts to contract again to reach its minimal radius shortly after minimum light. Although velocities in the atmosphere are low, we are aware that the atmosphere is not static at any point during the stars pulsation, which is contrary to what is assumed in most model atmosphere codes. But there are phases where the dynamical effects are smaller. These are the

¹ IRAF (<http://iraf.noao.edu/>) is distributed by the National Optical Astronomy Observatory, which is operated by the Association of Universities for Research in Astronomy (AURA) under cooperative agreement with the National Science Foundation.

Table 1. Basic data of the observations of RR Lyr.

Spectrum ID number	HJD – 2453000	Pulsational phase	Blazhko phase	SNR per pixel	Exposure time (s)
087	183.7953	0.173	0.280	293	960.000
088	183.8147	0.207	0.281	250	960.000
089	183.8271	0.229	0.281	172	960.000
091	183.8441	0.260	0.281	149	960.000
119	184.7293	0.820	0.304	215	960.000
120	184.7434	0.846	0.305	253	960.000
121	184.7559	0.868	0.305	271	960.000
122	184.7683	0.890	0.305	194	960.000
124	184.7865	0.922	0.306	162	960.000
125	184.7988	0.943	0.306	126	960.000
126	184.8121	0.967	0.306	63	960.000
158	185.7401	0.604	0.330	101	960.000
159	185.7523	0.626	0.331	126	960.000
160	185.7645	0.647	0.331	171	960.000
161	185.7768	0.669	0.331	233	960.000
163	185.7937	0.698	0.332	232	960.000
164	185.8059	0.720	0.332	259	960.000
165	185.8182	0.741	0.332	113	960.000
166	185.8304	0.763	0.333	210	960.000
168	185.8465	0.792	0.333	228	960.000
169	185.8587	0.814	0.333	290	960.000
170	185.8709	0.834	0.334	236	960.000
171	185.8831	0.856	0.334	216	960.000
173	185.8989	0.885	0.334	236	960.000
174	185.9112	0.905	0.335	215	960.000
175	185.9234	0.928	0.335	233	960.000
176	185.9356	0.948	0.335	290	960.000
178	185.9512	0.977	0.336	357	960.000
204	186.7293	0.349	0.356	190	960.000
205	186.7425	0.372	0.356	138	960.000
206	186.7548	0.394	0.356	203	960.000
207	186.7670	0.416	0.357	46	960.000
209	186.7876	0.452	0.357	131	960.000
210	186.8007	0.475	0.358	77	960.000
251	187.7208	0.098	0.381	359	960.000
252	187.7330	0.120	0.382	319	960.000
253	187.7442	0.141	0.382	120	769.397
255	187.7632	0.173	0.382	124	960.000
256	187.7803	0.203	0.383	160	960.000
257	187.7923	0.226	0.383	87	797.949
258	187.8060	0.249	0.383	272	960.000
260	187.8226	0.278	0.384	322	960.000
261	187.8370	0.303	0.384	214	960.000
262	187.8504	0.327	0.385	288	960.000
263	187.8634	0.349	0.385	216	960.000
319	243.6989	0.854	1.824	27	960.000
322	243.7688	0.976	1.826	21	960.000
323	243.7832	0.002	1.826	18	960.000
324	243.7955	0.024	1.827	18	960.000
326	243.8123	0.053	1.827	21	960.000
327	243.8262	0.078	1.827	25	960.000
328	243.8395	0.101	1.828	13	960.000
363	244.6062	0.454	1.847	231	960.000
364	244.6201	0.478	1.848	251	960.000
365	244.6323	0.500	1.848	258	960.000
366	244.6445	0.521	1.848	238	960.000
368	244.6622	0.553	1.849	249	960.000
369	244.6744	0.574	1.849	181	960.000
370	244.6870	0.596	1.849	173	960.000
371	244.6992	0.618	1.850	171	960.000
373	244.7168	0.648	1.850	152	960.000
374	244.7290	0.670	1.851	122	960.000
375	244.7412	0.693	1.851	90	960.000
376	244.7535	0.713	1.851	69	960.000

The first column shows the spectrum ID number and the second the Heliocentric Julian Date (HJD-2453000) at the beginning of the exposure. The third and fourth columns show the pulsational and Blazhko phase respectively for each observation. The fifth column shows the SNR per pixel calculated at $\sim 5000 \text{ \AA}$, while the sixth column shows the exposure time, in seconds, for each observation. The spectra number 253 and 257 have a lower exposure time, because the observation was stopped due to the presence of thick clouds. Spectrum number **260** is the one analyzed in detail in this paper.

phases we are interested in for abundance analysis. Note that the

pulsation model does not take into account the Blazhko modulation in the star.

3.2. The model atmosphere

To compute model atmospheres of RR Lyr, we employed the LLMODELS stellar model atmosphere code (Shulyak et al. 2004). For all the calculations, Local Thermodynamical Equilibrium (LTE) and plane-parallel geometry were assumed. Both these assumptions need to be discussed in our particular case.

The *LTE assumption* may be questionable due to low plasma density and shock waves in the RR Lyr atmosphere. To reduce the uncertainties of spectroscopic analysis we implement our model atmospheres at phases where the dynamical effects in the star’s atmosphere are expected to be small. We refer the reader to the next section for more explanations. Ignoring LTE may also lead to systematic errors in the abundance analysis. However, a detailed non-LTE analysis is beyond the scope of the present paper.

Atmospheres of giants are extended due to large radii and thus sphericity effects may become important for the stellar atmosphere modelling. For instance, based on detailed model atmosphere analysis Heiter & Eriksson (2006) recommended using spherically symmetric models for abundance analysis of stars having $\log g \leq 2$ and $4000 \text{ K} \leq T_{\text{eff}} \leq 6500 \text{ K}$. Taking into account the estimated gravitational acceleration of RR Lyr of $\log g = 2.4$ (see next section) one can expect the sphericity effects to be small enough to not significantly influence the abundance analysis. Indeed, the estimated errors of the Fe abundance based on theoretical Fe I lines presented in Heiter & Eriksson (2006) do not exceed 0.1 dex for the model with $T_{\text{eff}} = 6500$, $\log g = 1$. A $\log g = 2.4$ value for RR Lyr thus justifies the use of *plane-parallel model atmospheres* for abundance analysis.

We used the VALD database (Piskunov et al. 1995; Kupka et al. 1999, Ryabchikova et al. 1999) as a source of atomic line parameters for opacity calculations with the LLMODELS code. Finally, convection was implemented according to the Canuto & Mazzitelli (1991a,b) model of convection (see Heiter et al. (2002) for more details).

4. The optimal phase

During the pulsation cycle the spectral lines of RR Lyr change dramatically. In particular, when a shock wave passes through the atmosphere, it is possible to observe line broadening, line doubling, line disappearance, and sometimes even line emission (Preston et al. 1965, Chadid & Gillet 1996, Chadid et al. 2008, Preston 2009). This is obviously the sign of a very non-quietest atmosphere, that in principle cannot be modelled with a static model atmosphere, such as ATLAS and LLMODELS. In practice a model atmosphere code that is able to realistically model the atmosphere of a variable star such as RR Lyr, given both its chemical and pulsational peculiarity, does not yet exist. Therefore we are forced to use a static model atmosphere. In order to analyse the star in the most consistent way, we decided to study RR Lyr when its atmosphere is as close as possible to that of a non-variable star.

In the past, RR Lyrae stars were always analysed through spectra obtained close to the phase of minimum light because it was believed that this was the phase at which the star’s atmosphere is “at its quietest”. The adoption of static model atmospheres for the analysis of RR Lyrae stars was then justified through showing that the results obtained at different phases

were all in agreement with each other. At the “quiescent phase” we generally suppose that a) there are no shock-waves or any other fast plasma motions in the atmosphere that distort the line profiles and b) pressure stratification is as close as possible to its hydrostatic analog.

Picturing a homogeneously pulsating sphere, the most quiescent phase is associated with both phases of minimum and maximum radius. In case of an oversimplified pulsation model, these also correspond to the minimum and maximum light in the star’s luminosity variation. At these extreme positions in the pulsation, the atmosphere comes to a halt and, due to zero gas velocity, the pressure stratification at these phases is closest to the hydrostatic case (but not necessarily the same!). Furthermore, since the plasma velocities are negligible, the kinetic energy should be zero as well. For RR Lyrae stars, and especially those of type RRab (fundamental mode pulsators) with strongly nonlinear light curves (resembling a saw-tooth function), the phase of maximum light is short-lived and known to be accompanied by shock-waves. Thus, in previous works the quiescent phase was associated with the phase of minimum light. However, the assumption that all atmospheric layers move synchronously as being rigidly bound to each other is wrong. Realistic models show that at minimum radius, radiation is blocked in deeper layers and ready to migrate into the outer layers and accelerate both the photosphere and the atmosphere.

Looking at both pulsational models and a large sample of stellar spectra, obtained at different phases, we found that there is a quiescent phase very close to the phase of maximum radius, where the radial velocity derived from the metallic lines corresponds to the stellar gamma velocity. On the light curve this corresponds to a phase on the descending branch of the light variation. Figure 1 shows the calculated bolometric light curve, the photospheric radius variation, and the atmospheric kinetic energy as a function of the pulsation phase. The two vertical lines correspond to the phases of maximum stellar radius and of minimum light. As mentioned above the expansion of the model envelope is not homologous. We see different waves running in and out – some even steepening to shock waves.

Minimum light is a less fortunate choice to obtain undistorted line profiles, as parts of the atmosphere still move with supersonic speed (e.g., Mach 3 in Fig. 2). Fig. 2 shows radial plots covering approximately the outer 270 (of 400 total) radial mesh points in the Vienna pulsation model. For the phase of maximum radius and the phase of minimum light the gas velocity u (in units of the local sound) speed is plotted. At maximum radius (left panel in Fig. 2) the photosphere starts to move towards the model’s center, while parts of the envelope still move outwards. All velocities are below sound speed. At minimum light (right panel in Fig. 2) – which occurs before minimum radius – we see the transition between super- and subsonic inflow, sometimes called a shock, at the photosphere. This distorts the spectra and makes them less suited for our detailed analysis.

Note that the most quiescent phase, i.e. the phase of maximum radius, is actually very short-lived. A spectroscopic observation has to be well-timed (within, say, half an hour) in order to catch the spectral lines without distortion. Also, the integration times cannot exceed a few percent of the pulsation period, in order to avoid smearing of the spectra due to pulsation-induced Doppler effect. Integration times not much longer than 15 minutes taken within the appropriate (narrow) phase interval are recommended. This implies constraints on the obtained signal-to-noise ratio, and therefore, this study could only be done with +2-m telescopes. At minimum light the star is not at its quietest, and the shock wave associated with the bump phase (Gillet &

Crowe 1988) close to minimum light will also distort the spectral line profiles in RRab stars.

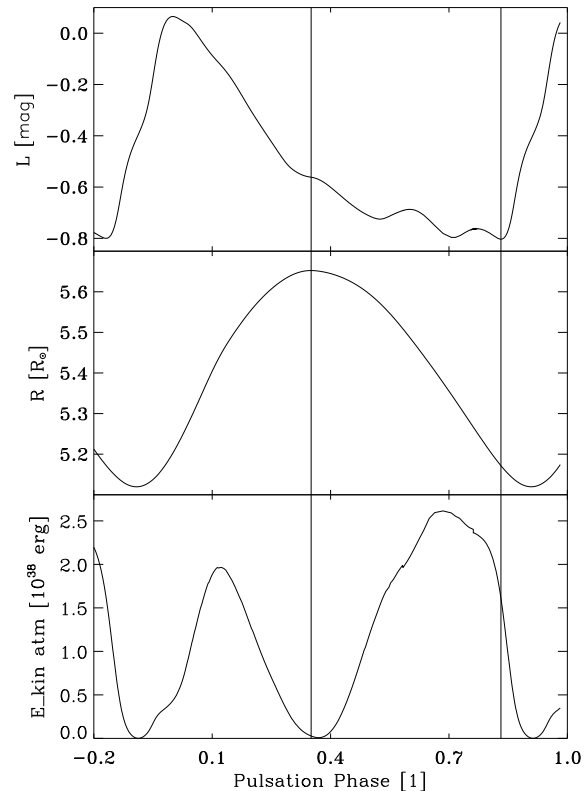


Fig. 1. RR Lyr model bolometric luminosity (upper panel), photospheric radius (middle panel), and atmospheric kinetic energy (lower panel) as a function of the pulsational phase. As convention phase 0 corresponds to the maximum of the luminosity. The two full vertical lines correspond to the phases of maximum radius (the phase we declare as most quiescent) and of minimum light (usually adopted for the spectroscopic analysis).

Fig. 1 shows clearly that the phase corresponding to minimum light occurs before a local minimum of the atmospheric kinetic energy, while at the phase of maximum radius the stellar atmosphere is very close to the other local minimum of kinetic energy.

This picture is also confirmed by the observations. Figure 3 shows the comparison of the line profile of RR Lyr in the region around 4500 Å and the bisector of the Ti II line at ~4501 Å as observed at the phases close to maximum radius and to minimum light. The main difference between the two line profiles is given by the line broadening, which is an indicator of the atmospheric activity: to a quiet phase correspond narrow spectral lines.

The spectral line broadening as a function of phase is shown in Fig. 4. This figure displays the full width at half maximum (FWHM) measured for four strong spectral features as a function of the pulsational phase. For each of the four lines we obtained a clear minimum close to the phase of maximum radius (between 0.2 and 0.3). This plot also shows the rapid changes in the FWHM when the shock waves occur. The observed peaks

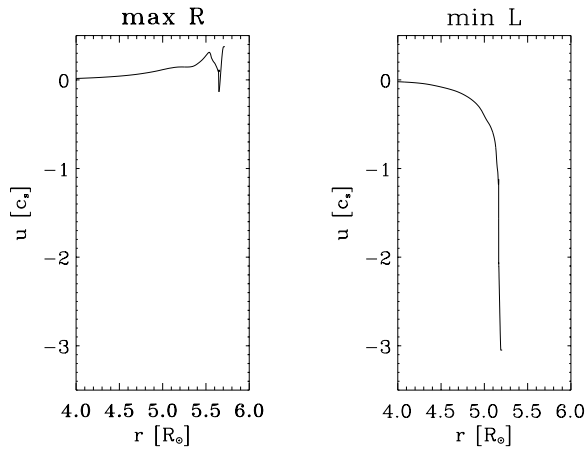


Fig. 2. Radial plots showing gas velocity u in units of the sound speed (the so-called Mach number) shown for the phase of maximum radius (left) and minimum light (right).

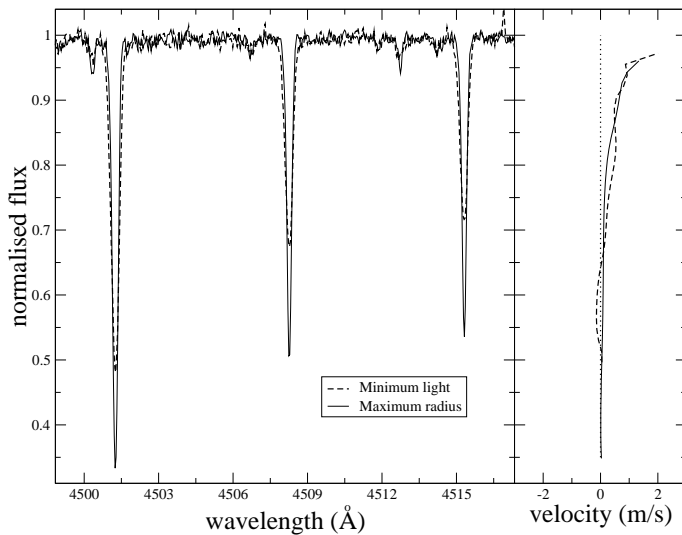


Fig. 3. Left panel: comparison between a part of the RR Lyr spectrum as observed close to the phase of maximum radius (full line) and close to the phase of minimum light (dashed line). Right panel: comparison between the bisectors of the Ti II line at ~ 4501 Å as observed close to the phase of maximum radius (full line) and close to the phase of minimum light (dashed line). The dotted line shows the zero velocity, for comparison. The velocity scale is in m s^{-1} .

in FWHM near pulsation phase ~ 0.65 and ~ 0.9 have been interpreted as arising from two shocks, a weaker and a stronger shock respectively, propagating through the star's atmosphere and producing compression of the turbulent gas (Fokin et al. 1999). Moreover, Fokin & Gillet (1997) and Fokin et al. (1999) showed that their RR Lyr models exhibit very strong shocks² up

² Fokin & Gillet (1997) note that the theoretical velocities and the shock amplitudes are very sensitive to model parameters. They used parameters different from ours: $T_{\text{eff}} = 7175$ K, $L = 62L_{\odot}$, $M = 0.578M_{\odot}$, $X = 0.7$ and $Y = 0.299$. The model generated with the Vienna Nonlinear Pulsation Code shows a maximum, during one pulsation cycle, of 4.7 Mach outward and -3.1 Mach inward, which correspond to gas velocities of 35 and -23 km/s. Due to artificial viscosity we can assume that

to Mach 25 in the highest part of the star's atmosphere (see Fig. 3 in Fokin et al. 1999).

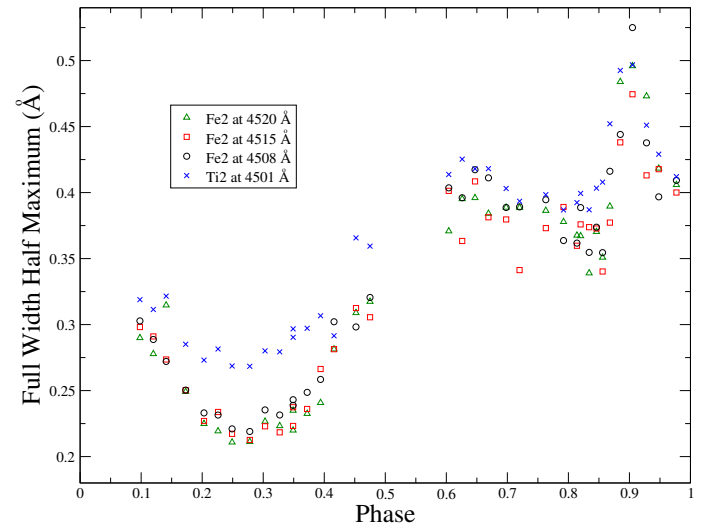


Fig. 4. Full width at half maximum (FWHM) in Å as a function of pulsational phase measured on three Fe II lines and one Ti II line. The minimum is in correspondance with the phase of maximum radius. The typical uncertainty on the FWHM is of ~ 0.01 Å, but it depends also on the SNR of each spectrum. The two peaks visible at about phase 0.65 and 0.9 are due to two propagating shock waves (Fokin et al. 1999).

The line bisectors, shown in Figure 3, also display that the line asymmetry changes with the pulsational phase. In particular, it has a trend similar to the one shown by the FWHM. This point will be described in more detailed in the next paper.

In practice it is not trivial to predict when the star will be at maximum radius exactly, due to the presence of the Blazhko effect and of other (possibly longer) periodicities involved in the pulsation. To find the appropriate spectrum for analysis, we investigated all the available spectra obtained close to the phase of maximum radius (determined with the simultaneous photometry) and picked the ones showing the minimum FWHM and line asymmetry. In the end the two spectra with numbers 258 and 260 were obtained very close to the phase of maximum radius and showed a comparable line broadening and a very small line asymmetry. We decided to perform a detailed analysis of spectrum number 260 because of its higher SNR. Our simultaneous photometry (Kolenberg et al. 2006) confirmed that this spectrum was recorded around pulsation phase $\phi = 0.28$.

5. Fundamental parameters and abundance analysis

In general a fundamental parameter determination begins from a derivation of T_{eff} and $\log g$ from photometric indexes. For RR Lyr this operation is not trivial. In Sect. 4 we assumed that

the star undergoes stronger shocks than our models. The artificial tensor viscosity used broadens the shock region and underestimates any possible heating phenomena. The position of the outer boundary condition is crucial in the maximum velocity, as shock waves steepen up when they run outwards towards smaller density. Fokin's model runs till $\rho = 10^{-14}$ while the Vienna models we used stop at about 10^{-10} .

the atmosphere of RR Lyr can be at best simplified as "static" only at the phase of maximum radius. Therefore it is at this phase that we made use of the photometric indices and the static model atmosphere grids to determine the fundamental parameters.

As starting point for our analysis we decided to take the parameters derived by other authors who analysed spectra of RR Lyr obtained at a similar phase. In particular Takeda et al. (2006) derived the fundamental parameters spectroscopically from high resolution spectra of RR Lyr, one of them obtained not far from the phase of maximum radius. These parameters can be taken only as starting point because the star was observed at a different Blazhko phase³. We will explore the effect of Blazhko modulation on the spectra of RR Lyr in our forthcoming work.

We used the parameters given by Takeda et al. (2006) for their spectrum taken at pulsation phase $\phi = 0.36$ ($T_{\text{eff}}=6040\pm 40$ K, $\log g=2.09\pm 0.1$ dex) as our starting point. We performed an iterative process to improve and test the parameters as described in the following. In our analysis, every time any of the parameters T_{eff} , $\log g$, ν_{mic} , or abundances changed during the iteration process, we calculated a new model by implementing the most recently determined quantities. We did the same with respect to the abundances. While the results of the abundance analysis depend upon the assumed model atmosphere, the atmospheric temperature-pressure structure itself depends upon the adopted abundances. We therefore recalculated the model atmosphere every time the abundances were changed, even if the other model parameters were kept fixed. This procedure ensured that the model structure was consistent with the assumed abundances.

5.1. The effective temperature

We performed the T_{eff} determination by fitting synthetic line profiles, calculated with SYNTH3 (Kochukhov 2007), to the observed profile of the H γ line, the only hydrogen line for which it was possible to make a reliable normalisation. In the temperature range expected for RR Lyr, hydrogen lines are very sensitive to temperature variations and depend very little on $\log g$ variations. In particular, this is expected when the stellar T_{eff} is close to its minimum. In the case of RR Lyr the use of hydrogen lines as T_{eff} indicators is very important because these lines describe the stellar structure more effectively than any other line, being formed in a wide region of the stellar atmosphere, and the line wings are free from non-LTE effects. The T_{eff} obtained with this procedure is $T_{\text{eff}} = 6125 \pm 50$ K. Note that these error bars are what we obtain from the fitting of the hydrogen line profile. As there are model uncertainties that are not taken into account in this fitting procedure, these error bars are probably underestimated. Figure 5 shows the comparison between the observed H γ line profile and the synthetic profiles calculated with the adopted stellar parameters, as well as the synthetic profiles obtained increasing and decreasing T_{eff} by 50 K.

Figure 5 shows a clear wavelength shift of the observed H γ core relative to its wings and to the metal lines formed in deeper layers. This is due to a velocity gradient in the outer layers of the star (Van Hoof & Struve 1953; Mathias et al. 1995 for RR Lyr).

Another spectroscopic indicator for T_{eff} is given by the analysis of metallic lines. In particular, T_{eff} is determined by eliminating the correlation between line abundance and line excitation potential (χ_{excit}) for a given ion/element. This procedure can lead

³ Fundamental parameters obtained at different Blazhko phases are not necessarily equal to one another, although they are obtained at the same pulsation phase.

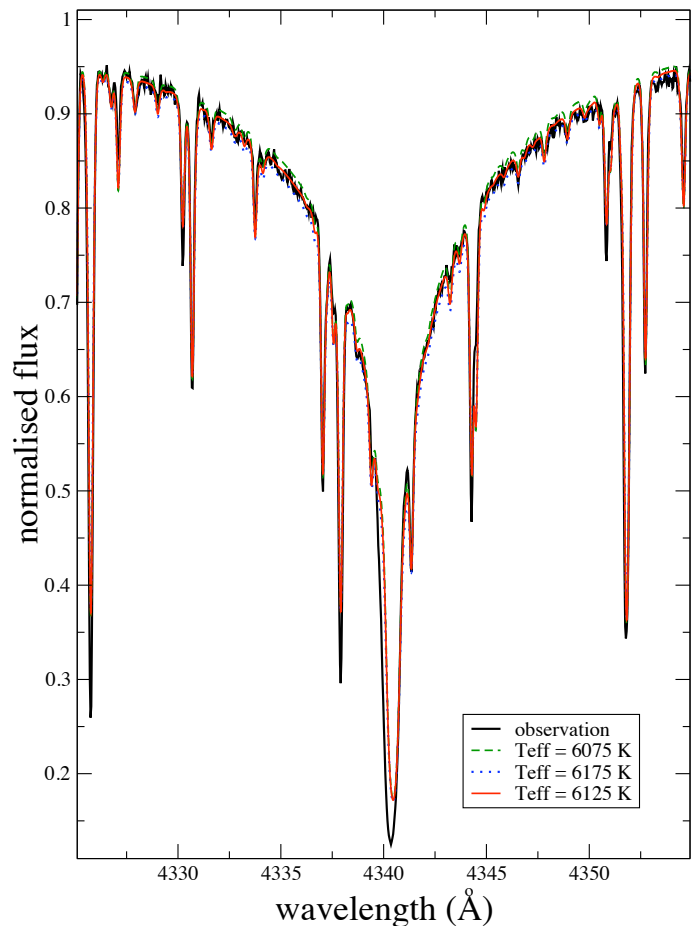


Fig. 5. Comparison between the observed H γ line profile (solid line) and synthetic profiles calculated with the final adopted $T_{\text{eff}}=6125$ K (red line) and with $T_{\text{eff}}=6175$ K (green line) and $T_{\text{eff}}=6075$ K (blue line). The red line agrees very well with the observed spectrum.

to erroneous parameters, in particular for stars such as RR Lyr where non-LTE effects could be large and the ν_{mic} determination is complicated by the pulsation (see Sect. 6.1). For this reason we decided not to take this indicator into account in our analysis, but to use it just as a check of the adopted T_{eff} value. This check pointed towards values comparable to the one we found from the H γ line profile fitting.

5.2. The surface gravity

The surface gravity can be derived using two independent methods: based on line profile fitting of gravity-sensitive metal lines with developed wings, and based on the ionisation balance of several elements. For RR Lyrae stars the Mg I lines are the most suitable lines for the first method. Described in Fuhrmann et al. (1997), the first method assumes that the wings of the Mg I lines at $\lambda\lambda$ 5167, 5172, and 5183 Å are very sensitive to $\log g$ variations. We decided to use this method only as a check on $\log g$ and not for parameter determination. The first reason for doing this is the large uncertainty in the $\nu \sin i$ and ν_{macro} values that, given the available spectral resolution and SNR, could not be precisely determined. Another reason is the slight line asymmetry (clearly visible for the strong lines, such as Mg I), which makes precise line profile fitting impossible. A third reason is the uncertainty

in the ν_{mic} value, that will be discussed in detail in Sect. 6.1. To make the comparison even more difficult there is the fact that the Mg abundance is about 1 dex below solar, making the wings of these lines not very pronounced.

The second method for surface gravity determination uses the assumption of ionisation equilibrium, but this method is extremely sensitive to the non-LTE effects present for each ion/element. Since we are not able to use the line profile fitting of the Mg I lines with developed wings, we rely on the ionisation equilibrium to determine $\log g$, checking the obtained result with the Mg I lines. In adopting the ionisation equilibrium, for some elements we took into account also the non-LTE corrections predicted by various authors on some specific elements in solar-type metal-poor stars. From the ionisation equilibrium we obtained $\log g = 2.4 \pm 0.2$. This value was derived using only the lines with an equivalent width of less than $75 \text{ m}\text{\AA}$, in order to minimise both the non-LTE effects and the uncertainty on the ν_{mic} (both more pronounced for the strong lines), and to assure a large enough number of lines, in particular for iron. We checked this value against the observed profiles of the Mg I lines with developed wings and obtained a good agreement, in particular when we adopt a depth-dependent ν_{mic} (see Sect. 6.1). For this comparison we used the line parameters of the Mg I lines adopted by Ryabchikova et al. (2009).

Our value for the surface gravity is supported by the ionisation equilibrium for Fe I/Fe II and few other elements, such as Si I/Si II and Ti I/Ti II. For Ca and V we do not obtain ionisation equilibrium, even within the error bars, but we have measured just one line for both Ca II and V I. Taking into account the non-LTE corrections for Ca I ($\sim +0.1-0.2$) and Ca II (almost in LTE) given by Mashonkina et al. (2006), ionisation equilibrium is achieved for that element. In the case of chromium, several Cr I and Cr II lines have theoretically calculated oscillator strengths, which may influence the final abundance results.

Since RR Lyr's effective temperature is too low to show enough He lines (though they are detected - see Preston 2009), we are unable to measure the atmospheric He abundance. Ryabchikova et al. (2009) tested the effect of a strong He depletion in the atmosphere of the solar type star HD 49933, concluding that a depleted He abundance would affect only the $\log g$ determination and leave T_{eff} unchanged within the error bars of 0.2 dex. We also tested the effect of a He overabundance for RR Lyr. If we assume $X = 0.5$ and $Y = 0.49$ we register a general abundance decrease, e.g. Fe decreases 0.3 dex. In addition, we observe a variation of the pressure sensitive features such as the Mg I lines with extended wings leading to changes in $\log g$ that do not exceed our error bars.

5.3. LTE abundance analysis

Our main source for the atomic parameters of spectral lines is the VALD database. LTE abundance analysis was based on equivalent widths, analysed with a modified version (Tsymbal 1996) of the WIDTH9 code (Kurucz 1993). We opted for equivalent widths because of the small line asymmetry and of the uncertainty on the form of the microturbulent velocity, making the synthetic line profile fitting more uncertain. We intend to analyse the other collected spectra of RR Lyr in the same consistent way. These spectra show a much more pronounced line asymmetry, therefore they will be analysed mostly through equivalent widths.

In total about 700 lines were measured with equivalent widths, but after a check against both the solar spectrum and

the spectrum of HD 49933 (Ryabchikova et al. 2009) we chose to keep 617 lines of 26 different elements and 32 different ions. We also tried to keep a set of lines uniformly distributed over the range of equivalent widths, wavelength, and excitation potentials, in particular for important ions such as Fe I for which we kept 284 lines. We used nearly all unblended spectral lines with accurate atomic parameters, except lines in spectral regions where the continuum normalisation was too uncertain. RR Lyr shows a strong underabundance for almost every measured ion/element. For this reason, it was possible to give only approximate abundance values or upper limits to the abundance of some ions for which it was not possible to calculate the equivalent width because of very weak lines. For these measurements we used synthetic line profile fitting, since these lines were too shallow to show both any visible line asymmetry and ν_{mic} dependence.

Microturbulence was determined by minimizing the correlation between equivalent width and abundance for several ions. We used mainly Fe I lines since this is the ion that provides the largest number of lines within a wide range in equivalent widths, but the correlations obtained with Ti I, Ti II, Cr I, Cr II, Fe II, and Ni I were also taken into account. Using all the available lines we could not find a unique value for the ν_{mic} able to completely remove the correlation between equivalent width and abundance. In particular it was possible to remove effectively this correlation using only the lines with an equivalent width of less than $75 \text{ m}\text{\AA}$, while the stronger lines exhibited a steep abundance increase with increasing equivalent width. Using only the lines with an equivalent width of less than $75 \text{ m}\text{\AA}$ we obtained a ν_{mic} of $2.4 \pm 0.3 \text{ km s}^{-1}$, while using all available lines we obtained a value of $3.1 \pm 0.5 \text{ km s}^{-1}$. In this last case the plot shows that the correlation is only statistically minimised (see lower plot of Fig. 6).

In the literature several authors mentioned the possibility of a depth-dependent ν_{mic} for RR Lyrae stars (Clementini et al. 1996, Takeda et al. 2006). Therefore, given the impossibility of finding a clear ν_{mic} value, we decided to derive the profile of a depth-dependent ν_{mic} using the available measured lines. This part of the work will be discussed in Sect. 6.1.

The full set of derived abundances, adopting both a constant and a depth dependent ν_{mic} is shown in Table 2. The last column of Table 2 gives the solar abundances by Asplund et al. (2005) for comparison.

The stellar metallicity (Z) is defined as follows:

$$Z_{\text{star}} = \frac{\sum_{a \geq 3} m_a 10^{\log(N_a/N_{\text{tot}})}}{\sum_{a \geq 1} m_a 10^{\log(N_a/N_{\text{tot}})}}, \quad (1)$$

where a is the atomic number of an element with atomic mass m_a . Making use of the abundances obtained from the performed analysis and assuming the depth-dependent ν_{mic} , we derived a metallicity of $Z = 0.003 \pm 0.002$ dex. For elements that were not analysed we adopted solar abundances from Asplund et al. (2005). However, if we assume an underabundance of -1.0 dex for all elements that were not analysed, excluding H and He, the resulting Z value remains practically unchanged. Note that in the pulsation model we used a metallicity value of $Z = 0.001$. This is on the lower border of the value we obtain from our spectrum. However, we have to keep in mind that we do not take into account NLTE effects in our analysis, and that these effects may influence our result. In general, for metal-poor stars such as RR Lyr, the NLTE correction is negative, meaning that the abundance in NLTE is lower, so the real Z would be lower too (from 0.003 more towards 0.001). The effect of NLTE on

Table 2. LTE atmospheric abundances for RR Lyr.

Ion	RR Lyr			Remarks	Sun
	$\log(N/N_{\text{tot}})$	$\log(N/N_{\text{tot}})$	n		$\log(N/N_{\text{tot}})$
C I	-4.84±0.04	-4.78±0.07	4		-3.65
N I	-4.77±0.11	-4.77±0.11	2	S	-4.26
O I	-3.98±0.04	-3.97±0.04	6	S	-3.38
Na I	-7.38±0.05	-7.38±0.05	2		-5.87
Mg I	-5.54±0.10	-5.48±0.14	8		-4.51
Al I	-6.59±0.26	-6.57±0.26	9	S	-5.67
Si I	-5.56±0.11	-5.55±0.11	10		-4.53
Si II	-5.61±0.04	-5.54±0.08	3		-4.53
S I	-5.94±0.08	-5.93±0.08	7	S	-4.90
K I	-7.81	-7.67	1		-6.96
Ca I	-6.98±0.05	-6.90±0.09	24		-5.73
Ca II	-6.71	-6.69	1		-5.73
Sc II	-10.17±0.13	-10.18±0.09	17		-8.99
Ti I	-8.33±0.08	-8.32±0.07	22		-7.14
Ti II	-8.21±0.19	-8.22±0.13	56		-7.14
V I	-9.64	-9.62	1		-8.04
V II	-9.22±0.09	-9.19±0.09	8		-8.04
Cr I	-7.98±0.09	-7.94±0.09	18		-6.40
Cr II	-7.70±0.11	-7.66±0.10	27		-6.40
Mn I	-8.47±0.15	-8.42±0.12	7		-6.65
Fe I	-6.07±0.12	-6.03±0.11	284		-4.59
Fe II	-5.93±0.13	-5.89±0.10	47		-4.59
Co I	-8.22	-8.21	1		-7.12
Ni I	-7.35±0.08	-7.33±0.08	38		-5.81
Cu I	-9.74	-9.73	1		-7.83
Zn I	-9.01±0.01	-8.99±0.01	2		-7.44
Ga I	-10.50	-10.50	2	UL/S	-9.16
Rb I	-9.75	-9.75	1	UL/S	-9.44
Sr I	-10.47	-10.46	1		-9.12
Sr II	-10.50	-10.48	1		-9.12
Y II	-11.31±0.09	-11.30±0.09	10		-9.83
Zr II	-10.56±0.07	-10.53±0.06	4		-9.45
Nb II	-11.50	-11.50	1	UL/S	-10.62
Mo I	-10.50	-10.50	1	UL/S	-10.12
Pd I	-11.00	-11.00	1	UL/S	-10.35
Ba II	-11.23±0.22	-11.35±0.08	5		-9.87
La II	-12.05±0.02	-12.05±0.02	3		-10.91
Ce II	-11.74±0.08	-11.73±0.08	8		-10.46
Pr II	-12.36±0.10	-12.35±0.10	16	S	-11.33
Nd II	-11.92	-11.91	1		-10.59
Sm II	-12.00±0.07	-12.00±0.07	10	S	-11.03
Eu II	-12.57	-12.55	1		-11.52
Gd II	-12.00±0.07	-12.00±0.07	5	S	-10.92
Tb II	-12.25±0.35	-12.25±0.35	2	S	-11.76
Dy II	-11.82±0.19	-11.80±0.19	6	S	-10.90
Ho II	-12.75±0.35	-12.75±0.35	2	S	-11.53
Er II	-11.61	-11.60	1		-11.11
Tm II	-12.50	-12.50	1	UL/S	-12.04
Lu II	-12.83±0.15	-12.83±0.15	3	S	-11.98
Hf II	-11.50	-11.50	1	UL/S	-11.16
Pb I	-11.00	-11.00	1	UL/S	-10.04
Tl II	-12.90	-12.90	1	UL/S	-11.95
T_{eff}	6125 K				5777 K
$\log g$	2.40				4.44
v_{mic}	3.1 km s ⁻¹	Depth dep.			0.875

Error bars are estimates based on the internal scatter from the number of analysed lines, n . The third column gives the atmospheric abundances in case of a polynomial depth dependent microturbulence velocity. The last column gives the solar abundance values from Asplund et al. (2005). The column indicated as "Remarks" shows whether the given abundance value is an upper limit (UL) and/or was obtained with synthetic spectra (S).

the abundances was illustrated by, e.g., Takeda et al. (2006) for oxygen. Using the solar Fe abundance value of Asplund et al. (2005), we obtain $[\text{Fe}/\text{H}] = -1.41 \pm 0.11$ for RR Lyr. This is in good agreement with the value $[\text{Fe}/\text{H}] = -1.39$ obtained by Beers et al. (2000), who list typical errors of 0.1–0.2 dex.

We used spectral synthesis with SYNTH3 to check the hyperfine structure (*hfs*) effects on the abundance determination of Mn, Cu, Zn, Ba, and Pr. For each measured line of each of these elements *hfs* effects are less than 0.01 dex, except for the Ba II line at λ 6141 Å for which the *hfs* correction is -0.1 dex, bring-

ing the line abundance closer to the mean Ba abundance. The *hfs* calculations for barium were taken from McWilliam (1998), who does not list the parameters for the Ba line at λ 6496 Å, but for this specific line we do not expect any significant *hfs* effect (Mashonkina & Zhai 2006).

The abundance uncertainties given in Table 2 are the standard deviation from the mean abundance (hence no uncertainties are given if the abundances were derived from a single line). More realistic error bars for each element/ion can be found in Ryabchikova et al. (2009) where a rigorous derivation of the abundance uncertainties is given on the basis of the adopted uncertainties on the stellar parameters. This direct comparison is possible because RR Lyr and HD 49933 have a similar T_{eff} and in particular similar values of the uncertainties on both T_{eff} and $\log g$.

Given the quality of the data and the slight line asymmetry it was not possible to give definite values for both $v \sin i$ and v_{macro} , but just to constrain their values. We obtained that $v \sin i$ lies between 0 and 9 km s⁻¹, and v_{macro} between 6 and 11 km s⁻¹. In particular with the minimum given $v \sin i$ we obtained the maximum v_{macro} and vice versa, as both effects contribute to line broadening. Note that the spectral lines cannot be fit with only the effects of rotational broadening ($v \sin i$). The constraints on $v \sin i$ that we obtained are in good agreement with the one obtained by Kolenberg (2002) through analysis of the line profile variations of the star. They also are in accord with the findings by Peterson et al. (1996), who measured the line widths for 27 RR Lyrae (of which 8 RRab) variables via cross-correlation analysis. They estimated an upper limit of 10 km/s for $v \sin i$ in all cases.

6. Discussion

6.1. A depth-dependent microturbulent velocity

As previously mentioned, we calculated the profile of a depth-dependent v_{mic} on the basis of the available equivalent widths obtained for several Fe I lines spanning a large range of values. A depth-dependent v_{mic} was previously suggested by several authors, such as Takeda et al. (2006), who found evidence that "strongly suggest that the microturbulence increases with height in the atmosphere of RR Lyrae stars, and that a simple application of the v_{mic} value derived from weak/medium-strength lines to stronger lines may result in an overestimation of the abundances".

Figure 6 displays the line abundance as a function of the measured equivalent width for all the measured Fe I lines in the spectrum of RR Lyr, calculated by assuming constant (bottom) and depth-dependent (middle) v_{mic} . It is clear that the use of a constant v_{mic} leads to an underestimation of the abundance of the medium-strength lines and an overestimation for the strong lines. In Fig. 6 we included as comparison the line abundance as a function of the measured equivalent width in HD 49933 for the set of common Fe I lines. This demonstrates that the observed behavior does not depend on the set of adopted lines.

We believe that this phenomenon could be explained both by strong non-LTE effects and by a depth-dependent v_{mic} . Generally speaking, non-LTE effects are stronger for deep lines compared to shallow lines and adopting line formation in LTE would lead to a higher abundance, in agreement with what we observe here. Gehren et al. (2001) showed that for solar-type stars there is a substantial Fe I underpopulation leading to stronger Fe line wings when assumed in LTE, while Fe II is in LTE, but Gehren et al. (2001) adopted a model atom for Fe that

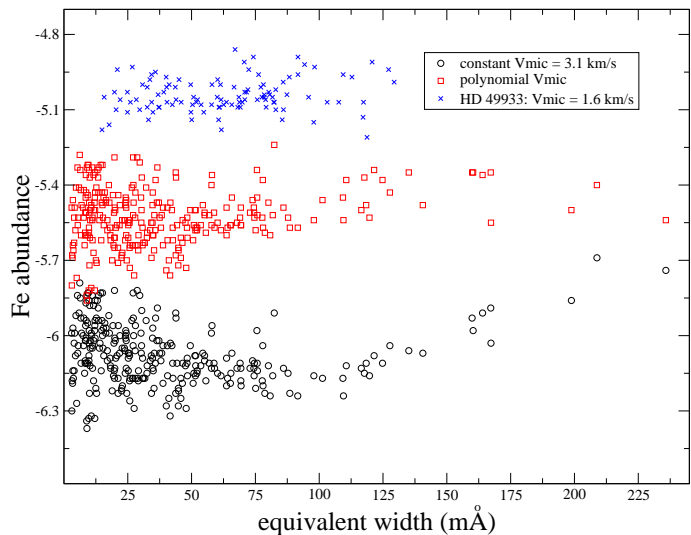


Fig. 6. Plots of individual abundances for 284 Fe I lines versus the measured equivalent width for RR Lyr, adopting a constant (open circles) and depth-dependent (open squares) v_{mic} . The same dependence for 108 common Fe I lines in the spectrum of HD 49933 is shown by crosses. We applied an arbitrary vertical shift for visualisation purposes.

did not include high-excitation levels. Mashonkina et al. (2009) analysed the Fe I/Fe II ionisation equilibrium in four solar-type stars and in the Sun concluding that the inclusion of the high-excitation levels in the Fe I model atom substantially reduced the non-LTE effects. RR Lyr is a metal poor giant for which non-LTE effects are expected to be stronger than in solar-type stars. If the deviation we register is due to non-LTE effects, it should only produce a deviation of about 0.5 dex for the stronger lines. We believe that the non-LTE effects are only partially responsible for the obtained deviation, because we observe it in all measured ions with a similar magnitude and always in the same direction. These ions include those for which non-LTE effects are supposed to be weak, such as Fe II, that shows deviations even stronger than those registered for Fe I. Note that non-LTE effects work differently for different ions, leading to deviations in both directions and with a wide range of magnitudes. For this reason we believe that a depth-dependent v_{mic} is mostly responsible for the observed deviations. A depth-dependent v_{mic} is also supported by modelling of RR Lyr stars as shown by Fokin et al. (1999) who observed pulsation-dependent variations in the microturbulent velocity (see their Fig. 3).

The depth-dependent v_{mic} profile was obtained fitting⁴ the line abundance in the plane equivalent width *versus* line abundance. We performed this procedure for Fe I, given the large number of measured lines and then tested the solution with the other ions. For each line the code searches the best individual line abundance, assuming a certain dependence of the microturbulent velocity on the atmospheric depth. This dependence is varied to minimise the dispersion between the observed and the theoretical line widths over the whole set of measured spectral lines. As the equivalent widths come from lines which are formed in a small fraction of the stellar atmosphere, it is impos-

sible to obtain a v_{mic} value at each atmospheric depth. For this reason it was necessary to speculate about the analytic form of the v_{mic} dependence on the atmospheric depth. We tested both a step-like function and a low-degree polynomial function. We chose the latter due to the unrealistically steep and large step needed for the step-like function.

Figure 7 shows the profile obtained for the depth-dependent v_{mic} in comparison with the sound speed calculated by LLMODELS. According to the results of Fokin et al. (1999) the v_{mic} should always be subsonic, due to the presence of strong dissipation effects. In Fig. 7 this is the case, except for the region between $\log \tau_{5000}$ equal to -3.5 and -5.5 v_{mic} where v_{mic} becomes supersonic. This, however, should be interpreted with caution since the numeric calculation of the sound speed with the LLMODELS code may suffer from accuracy loss in uppermost layers where the thermodynamic variables (like pressure and density) are slowly changing functions with atmospheric depth. Also notice that our empirical estimation of the v_{mic} may contain systematic uncertainties, and thus the supersonic regime shown in Fig. 7 may have little to do with reality. Nevertheless, the general behavior of v_{mic} with depth (i.e., strong increase in superficial layers) plausibly reflects a real physical phenomenon.

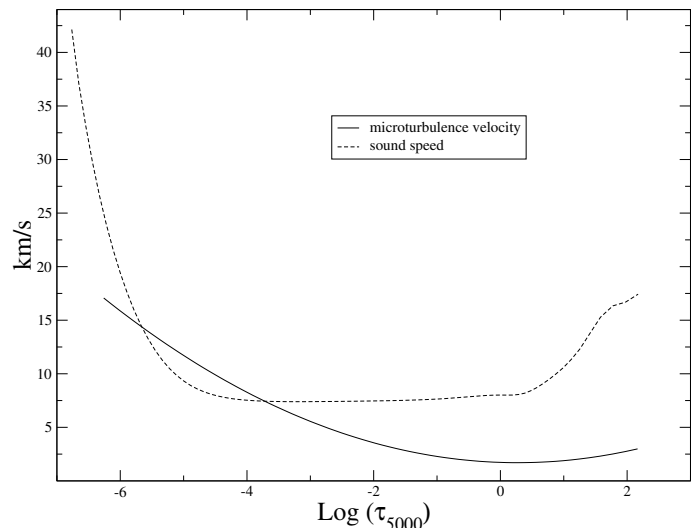


Fig. 7. Comparison between the profile of the microturbulent velocity (full line) and of the sound speed (dashed line) as a function of atmospheric depth.

Assuming a depth-dependent v_{mic} the abundances of most ions change, in particular the ones with a large number of strong lines. As expected, for most of the ions the abundance increases instead of decreasing. This phenomenon is explained by the fact that our adopted value of constant v_{mic} is overestimated because it was obtained by minimising statistically the correlation abundance *versus* equivalent width. Because we have a large number of middle-strength lines, a small number of strong lines and an overestimated v_{mic} we obtained an underestimated abundance (see the bottom plot of Fig. 6). When applying the depth-dependent v_{mic} , the middle-strength lines (responsible for the underestimated abundance) yield an abundance similar to the shallow and strong lines, thus leading to a higher final abundance. This effect is visible for ions with a large number of lines, such as Fe I. Instead, for elements with few lines and some of

⁴ The code adopts an LTE plane-parallel model atmosphere calculated using subroutines of the SynthV code (Tsymbal 1996) and the DUNLSF minimisation procedure of the IMSL numerical libraries package.

them very strong, such as Ba II, the final abundance decreases, with a considerable decrease of the standard deviation as well.

6.2. Comparison with previous determinations

Since we propose a different approach to the analysis of RR Lyrae stars with the aim of determining their physical parameters, it is important to compare our results with what was previously obtained by other authors. The main publications on this topic containing an abundance analysis and parameter determination of RR Lyr itself are Clementini et al. (1995), Lambert et al. (1996), and Takeda et al. (2006).

Clementini et al. (1995) analysed several field RR Lyrae stars to derive broad band photometric calibrations for both fundamental parameters and metallicity. Their spectra of RR Lyr covered a large wavelength range with a moderate resolution ($R \sim 38\,000$) and a high SNR (probably assumed per pixel) of about 460. They observed RR Lyr at pulsational phases of 0.70 and 0.73, around minimum light. Since they did not find any systematic difference between the two spectra they summed them to get one high-SNR spectrum. They compare the T_{eff} value obtained from broad band photometry by several other authors between 1975 and 1994, and, taking into account these comparisons, they build their own calibration leading to a T_{eff} value of 6222 ± 115 K. They derive the surface gravity from the stellar mass and radius, obtaining a $\log g$ value of 2.8 ± 0.2 dex. The microturbulent velocity was derived in the usual way (minimisation of the correlation between line abundance and equivalent widths) obtaining a value of 4.2 ± 0.2 km s⁻¹. Clementini et al. (1995) also mention the possibility of a depth-dependent v_{mic} , but they concluded that, if present, a v_{mic} depth-dependency is only very small and affects the abundances by just 0.1 dex (0.2 dex for the elements with a large number of strong lines). We confirm this estimate with our present work (see Table 2). Most of their abundances are in LTE, except for oxygen and sodium that were analysed in non-LTE. Table 3 shows a comparison between the abundances obtained by Clementini et al. (1995) and the ones derived in this work. The comparison shows a rather good general agreement between the two sets of abundances, where for only Al I, Sc II, Mn I and Zn I we register a small disagreement.

Lambert et al. (1996) observed a set of RR Lyrae stars with a spectral resolution of 23 000 to obtain narrow and broad band photometric calibrations for fundamental parameters and metallicity. RR Lyr was observed at eight different phases, one of them close to the phase of minimum light and one close to the phase of maximum radius. The spectrum obtained close to the phase of maximum radius has a SNR (assumed per pixel) of ~ 100 . For each phase they derived the fundamental parameters both from photometry (adopting previously existing calibrations) and from spectroscopy. From the photometric calibration they obtained, for the spectrum at phase close to maximum radius, $T_{\text{eff}} = 6350 \pm 200$ K and $\log g = 2.6 \pm 0.2$ dex, while from spectroscopy they derived $T_{\text{eff}} = 6200 \pm 200$ K and $\log g = 2.3 \pm 0.2$ dex. Lambert et al. (1996) found a constant v_{mic} along the stellar atmosphere, but the most surprising result is that they obtained also a rather constant v_{mic} along the pulsational phase (between 3.6 ± 0.3 km s⁻¹ and 4.4 ± 0.5 km s⁻¹). This result is surprising given the fact that several pulsation models of RR Lyrae stars show large variations of the v_{mic} along the pulsational cycle. We will study this issue in detail in the forthcoming work. In general the high value obtained by Lambert et al. (1996) shows the turbulent motions present in the atmosphere and it fits with the large value we also obtained when a constant v_{mic} is assumed. Lambert et al. (1996) derived the Ca and Fe abundance both in

Table 3. Comparison between the atmospheric ion abundances relative to the Sun obtained by Clementini et al. (1995) and in this work.

Ion	$[N_{\text{el}}/N_{\text{H}}]_{\text{Sun}}$		Clementini et al. (1995)
	This work		
O I	-0.60 ± 0.04	-0.59 ± 0.04	-0.69
Na I	-1.51 ± 0.05	-1.51 ± 0.05	-1.39
Mg I	-1.03 ± 0.10	-0.97 ± 0.14	-1.08 ± 0.07
Al I	-0.92 ± 0.26	-0.90 ± 0.26	-1.89
Si I	-1.03 ± 0.11	-1.02 ± 0.11	-0.92 ± 0.02
Si II	-1.08 ± 0.04	-1.01 ± 0.08	-1.14
Ca I	-1.25 ± 0.05	-1.17 ± 0.09	-1.07 ± 0.05
Sc II	-1.18 ± 0.13	-1.19 ± 0.09	-1.35 ± 0.12
Ti I	-1.19 ± 0.08	-1.18 ± 0.07	-1.20 ± 0.06
Ti II	-1.07 ± 0.19	-1.08 ± 0.13	-1.05 ± 0.18
Cr I	-1.58 ± 0.09	-1.54 ± 0.09	-1.41 ± 0.18
Cr II	-1.30 ± 0.11	-1.26 ± 0.10	-1.33 ± 0.14
Mn I	-1.82 ± 0.15	-1.77 ± 0.12	-1.99 ± 0.12
Fe I	-1.48 ± 0.12	-1.44 ± 0.11	-1.39 ± 0.13
Fe II	-1.34 ± 0.13	-1.30 ± 0.10	-1.39 ± 0.13
Ni I	-1.54 ± 0.08	-1.52 ± 0.08	-1.47
Zn I	-1.57 ± 0.01	-1.55 ± 0.01	-1.35
Y II	-1.48 ± 0.09	-1.47 ± 0.09	-1.50
Ba II	-1.36 ± 0.22	-1.48 ± 0.08	-1.39 ± 0.12
v_{mic}	3.1 km s ⁻¹	Depth dep.	4.2 km s ⁻¹

The second and third column show the abundances relative to the Sun obtained in this work, while the fourth column lists the abundances relative to the Sun published by Clementini et al. (1995).

LTE and non-LTE, adopting only the lines that are not deeper than 100 mÅ. In LTE they obtained $\log(N_{\text{Fe}}/N_{\text{tot}}) = -6.06$ dex and $\log(N_{\text{Ca}}/N_{\text{tot}}) = -6.89$ dex. In non-LTE they obtained a correction of about 0.2 dex for Fe I and no correction for Fe II, but, as mentioned in Sect. 6.1, we believe that the non-LTE correction for Fe I is much smaller. The non-LTE correction they obtained for Ca I was ~ 0.05 dex. Both the Fe and Ca abundance presented by Lambert et al. (1996) are in good agreement with what we obtained. There is the possibility that the higher T_{eff} and v_{mic} relative to what we adopted compensate each other leading to values very close to the ones obtained with a lower T_{eff} and v_{mic} .

Takeda et al. (2006) analysed five spectra of RR Lyr with the aim to derive spectroscopically the fundamental parameters and the abundances of O, Si, and Fe. The spectra were obtained in high resolution ($R \sim 60\,000$) with a rather high SNR (~ 350 – 400), but in a very limited wavelength range intended to cover mainly the oxygen triplet at $\lambda\lambda \sim 7770$ Å. One of these five spectra was obtained at a pulsational phase close to the phase of maximum radius. The fundamental parameters were derived minimising the correlation between line abundance and excitation potential (T_{eff}) and with the ionisation equilibrium ($\log g$). The hydrogen line wings were used as check of the parameters determined, the inverse of the strategy we applied. For this phase they obtained $T_{\text{eff}} = 6040 \pm 40$ K, $\log g = 2.09 \pm 0.1$ dex, and $v_{\text{mic}} = 3.0 \pm 0.1$ km s⁻¹. The v_{mic} value obtained by Takeda et al. (2006) is in very good agreement with what we have found using a constant v_{mic} . They also strongly suggest the presence of a depth-dependent v_{mic} for RR Lyrae stars. Takeda et al. (2006) analysed two sets of oxygen lines in non-LTE obtaining two values for the O abundance of -4.11 dex and -4.00 dex. We believe that the difference between their two obtained values is due to the fact that they adopted a constant v_{mic} . The strong infrared oxygen triplet is very sensitive to the adopted v_{mic} . The O abundance we obtained is very close to -4.00 dex assuming both a constant and a depth-dependent v_{mic} . Takeda et al. (2006) also derived the Si and Fe abundance in LTE, obtaining respectively -5.93 dex and -5.82 dex. These two values do not match very well our results (we obtain a higher Si

abundance and a lower Fe abundance). We are not able to explain this difference since it cannot be due to the small differences in the adopted stellar parameters.

The effective temperatures determined in these studies may not be directly comparable because the analysed spectra were obtained at different Blazhko phases. A more reasonable comparison can be done for the surface gravity because it is supposed to change less during the pulsation cycle.

What clearly emerges is a systematic difference between the $\log g$ obtained from stellar mass and radius and from the ionisation equilibrium. The ionisation equilibrium leads to a lower $\log g$ compared to what was derived by the assumed stellar mass and radius. Our $\log g$ value lies in between and it is well validated from the fit of the magnesium lines with developed wings. This method is independent of both the ionisation equilibrium and the assumed stellar mass and radius.

The other parameters that can be directly compared are the elemental abundances. We do not expect those to vary within the pulsation cycle, unless the pulsation is able to bring material from the inner core up to the stellar atmosphere, a possibility that we find unlikely. Comparing the abundances obtained in the three previous studies and in our work, we note good agreement except for a few exceptions. This means that there is the actual possibility that if static models can be applied to RR Lyrae stars, they can be applied to many phases (not all!), but we will tackle this issue in our next work on the analysis of the other acquired spectra of RR Lyr.

From the point of view of the atmospheric modelling, the main difference between earlier work and ours is the adoption of an abundance-dependent model atmosphere for an RR Lyrae type star. The impact of depth-dependent microturbulent velocity and individual chemistry is shown in Fig. 8. As expected, strong underabundance makes the temperature in the surface layers higher compared to solar or scaled solar models. Introduction of the depth-dependent v_{mic} affects the strongest spectral features, leading to weaker absorption at their line center. This, in turn, decreases the line absorption coefficient and thus leads to a further increase of the temperature. For instance, the temperature difference between models computed with constant and depth-dependent microturbulent velocities (see Fig. 7) can amount to as much as 300 K. On the other hand, only the strongest lines feel this modification in model temperature structure and thus the statistical results of abundance analysis are not affected that much, as shown in Table 2.

In contrast, line profile analysis of strong lines must be performed with appropriate models that account for the effect of depth-dependent microturbulence. Finally, we do not find any noticeable difference in temperature structure between the scaled-solar model ($[M/H]=-1.5$), which corresponds to the mean underabundance we found for Fe, and individual abundance models. This allows us to use scaled abundance models to mimic the temperature structure of the star as a first guess. Note however that metallicity is the result of abundance analysis, which is not known in the beginning. This methodological difficulty is automatically removed using an iterative procedure of abundance analysis as applied in this study.

7. Conclusions

Fundamental-mode RR Lyrae (RRab) stars pulsate with high velocities which, in certain phases, leads to a distortion of their spectral features. The aim of the study presented in this paper was to determine a set of self-consistent and accurate parameters and abundances for RR Lyr, the prototype and brightest

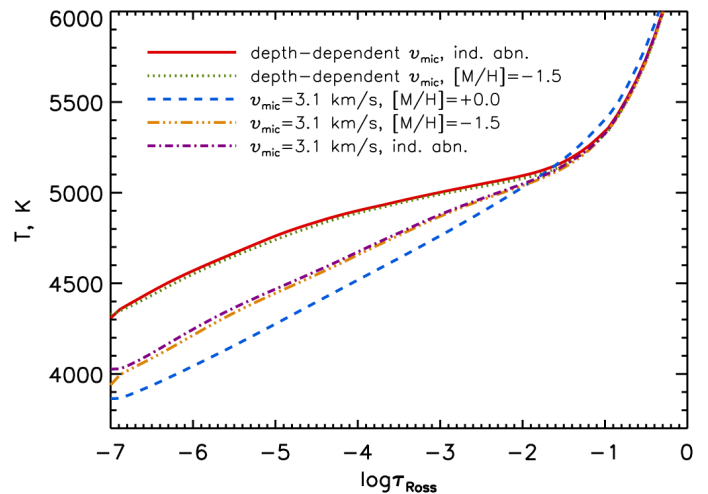


Fig. 8. Comparison of temperature structures of models computed under different assumptions about microturbulent velocity v_{mic} and abundances (see the legend on the plot). Depth-dependent v_{mic} was taken from Fig. 7. For all the models we took $T_{\text{eff}}=6125$, $\log g=2.4$.

member of its class. For this, we had a set of high-resolution spectroscopic data at our disposal, obtained with the Robert G. Tull Coudé Spectrograph on the 2.7-m telescope of McDonald Observatory. In order to derive the most reliable abundances for the star, we determined the phase in RR Lyr’s pulsation cycle at which the atmosphere is “at its most quiescent”, the phase of maximum radius. Our assumptions were strengthened by the Vienna Nonlinear Pulsation Code. With observations taken at the phase of maximum radius, the fundamental parameters and the element abundances of RR Lyr were determined through an iterative process. For the determination of the effective temperature, we used synthetic line profile fitting to the H γ line and obtained $T_{\text{eff}} = 6125 \pm 50$ K (error bars from the fitting procedure only). For the $\log g$ determination we used the condition of ionisation equilibrium and obtained a $\log g$ value of 2.4 ± 0.2 at the phase of maximum radius. The LTE abundance analysis based on element abundances *versus* equivalent widths could not fit the element abundances with a single microturbulent velocity (v_{mic}) value. A depth-dependent v_{mic} is physically plausible for RR Lyrae atmospheres and was previously suggested (but never derived or quantified) by several authors. In this work, we derived, for the first time, the depth-dependent v_{mic} profile and quantified the expected abundance variation. With the depth-dependent v_{mic} we obtained a better agreement between the element abundances and equivalent widths. In general, the adoption of a fixed v_{mic} value (which is too high) leads to an underestimation of the element abundances by 0.06 dex (maximum value). Nevertheless, RR Lyr is shown to be underabundant in all heavy elements, in agreement with previous studies.

RR Lyr, the eponym of its class, is one of the best studied RR Lyrae stars. However, many intricacies of its pulsation remain poorly understood, and in order to accurately model the star, we have to take into account complex physics that we are only beginning to uncover. The star is an asteroseismic target of the *Kepler* Mission (Borucki et al. 2009) through the Kepler Asteroseismic Science Consortium (KASC, see also Gilliland et al. 2010). Besides the fact that the star displays amplitude and phase modulation (the so-called Blazhko effect), Kolenberg et al. (2010) recently detected, for the first time, the occurrence of

half-integer frequencies in the star, i.e., peaks at $\frac{1}{2}f_0$, $\frac{3}{2}f_0$, $\frac{5}{2}f_0$ etc., with f_0 the main pulsation frequency. This phenomenon (“period doubling”) may be caused by instabilities in the star and connected to the mysterious Blazhko effect (see Szabó et al. 2010, in preparation). In order to further explore theoretical models of RR Lyr, it is necessary to know the physical parameters of the star with the highest accuracy possible.

For this reason, an in-depth analysis of the star’s atmospheric motions is very timely. We intend to expand this analysis in our forthcoming publications of the star. Our study clearly illustrates that it is crucial to use the appropriate models to correctly interpret the spectral data of RR Lyrae stars, and that high-quality observations can contribute to improving those models.

Acknowledgements. We kindly thank the referee of this paper, Dr. George Preston, for constructive comments. KK is a Hertha Firnberg Fellow, supported by the Austrian Science Foundation (FWF project T359-N2 and FWF stand-alone project P19962). LF has received support from the Austrian Science Foundation (FWF project P19962). His research at the Open University (UK) is funded by an STFC Rolling Grant. DS is supported by Deutsche Forschungsgemeinschaft (DFG) Research Grant RE1664/7-1. OK is a Royal Swedish Academy of Sciences Research Fellow supported by grants from the Knut and Alice Wallenberg Foundation and the Swedish Research Council. We kindly thank Stefano Bagnulo and John Landstreet for the useful discussions and comments during the preparation of the draft.

References

- Asplund, M., Grevesse, N., & Sauval, A. J. 2005, *Astronomical Society of the Pacific Conference Series*, 336, 25
- Barklem, P. S., Stempels, H. C., Allende Prieto, C., et al. 2002, *A&A*, 385, 951
- Beers, T. C., Chiba, M., Yoshii, Y., Platais, I., Hanson, R. B.; Fuchs, B., Rossi, S., 2000, *AJ*, 119, 2866
- Benedict, G. F., McArthur, B. E., Fredrick, L. W., et al., 2002, *AJ*, 123, 473
- Borucki W. J., Koch D., Basri G. et al., 2010, *Science*, 327, 977
- Canuto, V. M., & Mazzitelli, I. 1991, *ApJ*, 370, 295
- Canuto, V. M., & Mazzitelli, I. 1992, *ApJ*, 389, 724
- Chadid, M. & Gillet, D. 1996, *A&A*, 308, 481
- Chadid, M., Vermin, J., Gillet, D., 2008, *A&A*, 491, 537
- Clementini, G., Carretta, E., Gratton, R., et al. 1995, *AJ*, 110, 2319
- Feuchtinger, M.U. 1999, *A&A*, 351, 103
- Fokin, A. B. & Gillet, D. 1997, *A&A*, 325, 1013
- Fokin, A. B., Gillet, D. & Chadid, M. 1999, *A&A*, 344, 930
- Fossati, L., Ryabchikova, T., Bagnulo, S., et al., 2009, *A&A*, 503, 945
- Fuhrmann, K., Pfeiffer, M., Frank, C., Reetz, J., & Gehren, T. 1997, *A&A*, 323, 909
- Gehren, T., Butler, K., Mashonkina, L., Reetz, J. & Shi, J. 2001, *A&A*, 366, 981
- Gillet, D., Crowe, R. A., 1988, *A&A*, 199, 242
- Gilliland R. L., Brown T. M., Christensen-Dalsgaard J. et al., 2010, *PASP*, 122, 131
- Juresik, J., Hurta, Zs., Sódor, Á., Szeidl, B., et al., 2009, *MNRAS*, 397, 350
- Heiter, U., Kupka, F., van’t Veer–Menneret, C., Barban, C., et al. 2002, *A&A*, 392, 619
- Heiter, U., Eriksson, K. 2006, *A&A*, 452, 1039
- Kochukhov, O. 2007, *Spectrum synthesis for magnetic, chemically stratified stellar atmospheres*, *Physics of Magnetic Stars*, 109, 118
- Kolenberg, K., Ph.D. Thesis, University of Leuven, http://www.ster.kuleuven.be/pub/kolenberg_phd/
- Kolenberg, K., Smith, H. A., Gazeas, K. D., et al. 2006, *A&A*459, L577
- Kolenberg, K., Szábo, R., Kurtz, D. W., Gilliland, R. L., et al. 2010, *ApJ*, 713, 198
- Kupka, F., Piskunov, N., Ryabchikova, T. A., Stempels, H. C., & Weiss, W. W. 1999, *A&AS*, 138, 119
- Kurucz, R. 1993, *ATLAS9: Stellar Atmosphere Programs and 2 km/s grid*. Kurucz CD-ROM No. 13 (Cambridge: Smithsonian Astrophysical Observatory)
- LaCluyzé, A., Smith, H. A., Gill, E.-M., et al. 2004, *AJ*127, 1653
- Lambert, D. L., Heath, J. E., Lemke, M. & Drake, J. 1996, *ApJS*, 103, 183
- Manduca, A., Bell, R. A., Barbes, T. G., et al., 1981, *ApJ*, 250, 312
- Mashonkina, L., Korn, A. J. & Przybilla, N. 2006, *A&A*, 461, 261
- Mashonkina, L. & Zhao, G. 2006, *A&A*, 456, 313
- Mashonkina, L., Gehren, T., Shi, J., Korn, A. & Grupp, F. 2009, *Fe I/Fe II ionization equilibrium in cool stars: NLTE versus LTE*, proceedings of IAU Symposium 265, *Chemical Abundances in the Universe: Connecting First Stars to Planets*, K. Cunha, M. Spite & B. Barbuy, eds, arXiv: 0910.3997
- Mathias, P., Gillet, D., Fokin, A. B., & Chadid, M., 1995, *ã*, 298, 843
- McWilliam, A. 1998, *AJ*, 115, 1640
- Peterson, R. C., Carney, B/ W., & Latham, D. W., 1996, *ApJ*, 465, 47
- Piskunov, N. E., Kupka, F., Ryabchikova, T. A., Weiss, W. W., & Jeffery, C. S. 1995, *A&AS*, 112, 525
- Preston, G. W., Smak, J., & Paczynski, B. 1965, *ApJS*, 12, 99
- Preston, G. W., 2009, *ã*, 507, 1621
- Przybilla, N., Butler, K., Becker, S. R., & Kudritzki, R. P. 2006, *A&A*, 445, 1099
- Ryabchikova, T. A., Piskunov, N. E., Stempels, H. C., Kupka, F., & Weiss, W. W. 1999, *Phis. Scr.*, T83, 162
- Ryabchikova, T. A., Fossati, L. & Shulyak, D. 2009, *A&A*, 506, 203
- Siegel, M. J., 1982, *PASP*, 94, 122
- Shulyak, D., Tsymbal, V., Ryabchikova, T., Stütz Ch., & Weiss, W. W. 2004, *A&A*, 428, 993
- Szeidl, B. 1988, in: *Multimode Stellar Pulsations*, Eds. G. Kovacs, L. Szabados and B. Szeidl, *Kultura*, 45
- Szabó, R., Kolláth, Z., Molnár, L. et al., 2010, in preparation
- Takeda, Y., Honda, S., Aoki, W., et al. 2006, *PASJ*, 58, 389
- Tody, D. 1993, in *ASP Conf. Ser. 52, Astronomical Data Analysis Software and Systems II*, ed. R. J. Hanisch, R. J. V. Brissenden, & J. Barnes (San Francisco: ASP), 173
- Tsymbal, V. V. 1996, in *ASP Conf. Ser. 108, Model Atmospheres and Spectral Synthesis*, ed. S. J., Adelman, F., Kupka, & W. W., Weiss, 198
- Van Hoof, A., & Struve, O. 1953, *PASP*, 65, 158